A Comprehensive Gridded Dataset Associated to the Climate Change Effect on the Water Resources in the Grand Est Region, France

Mărgărit-Mircea Nistor, Ionel Haidu, Ştefan Dezsi, Cristina Ştefan

atmosphere

MDPI

Article

A Comprehensive Gridded Dataset Associated to the Climate Change Effect on the Water Resources in the Grand Est Region, France

Mărgărit-Mircea Nistor [1,*,†], Ionel Haidu [2,†], Ştefan Dezsi [3,†] and Cristina Ştefan [4]

1 Department of Hydrogeology, Earthresearch Company, 400667 Cluj-Napoca, Romania
2 Laboratory LOTERR, EA-7304, University of Lorraine, 57045 Metz, France
3 Faculty of Geography, University of Babeş-Bolyai, 5–7 Clinicilor Street, 400006 Cluj-Napoca, Romania
4 Duke-NUS Global Health Institute (SDGHI), Duke-NUS Medical School, Singapore 169857, Singapore; cristinastefan10@gmail.com
* Correspondence: renddel@yahoo.com
† These authors contributed equally.

Received: 14 July 2020; Accepted: 22 September 2020; Published: 24 September 2020

Abstract: Water resources and environment quality are nowadays under high pressure because of climate change, land use practices, as well as human actions. A comprehensive gridded dataset becomes a necessary instrument to assess the risk level at regional scale, and also for territorial planning, the defining strategies to address future natural and anthropological challenges. In order to obtain a complete database with the most important parameters at spatial scale, this study is constructed as a preparation of layers used for various environmental risks, but mostly with the climate change effect on the water resources from the Grand Est region, France. In addition, geological formations, terrain data, and land cover were harmonized as grid format for the study area. Thus, the temperature and precipitation parameters, related to the 1961–1990 (1990s), 2011–2040 (2020s), and 2041–2070 (2050s), become useful data for evapotranspiration, water availability, and effective precipitation calculations. The geology layer indicates the composition and types of aquifers and it contributes to the potential infiltration map (PIM). The morphology of the terrain contributes to the slope angle and PIM. Through the typology of land cover, the pollution load index (PLI) was estimated. The findings indicate intense aridization and the depletion of the effective precipitation (below 650 mm) during the present and future periods. With respect to these concerns, the surface waters and groundwater resources from the Grand Est region are experiencing the negative effects of climate change on runoff and aquifers recharge respectively. In addition, the high PLI in the industrial and agricultural areas contribute to the possibility of the increasing water resources vulnerability. The affected areas extend mainly in the western, north-central, and north-eastern parts of the region, mainly in the Rhine, Aube, and Marne Valleys. Considered as a precious resource in the region, the water management should follow best practices for vulnerability and risk assessment, and further to delineate the protection areas. As a comprehensive gridded dataset, the calculations and original maps presented in this paper represent a complex product with main environmental parameters processed at spatial scale of 1 km^2 in ArcGIS. This product has the purpose to integrate the geospatial data for the Grand Est region of France.

Keywords: climate models; terrain morphology; hydrogeology; Geographical Information Systems (GIS); dataset; Grand Est

1. Introduction

Climate change and intensive land use for agriculture and resources extraction have shown to have, in most cases, a negative influence on the water resources and environment, in various places of the globe [**? ? ?**]. Often, the global and regional changes are related to improper management of the territory and to limitations in the action plans for natural resources conservation [**? ? ?**]. Climate change has definitely a negative impact on glaciers and water systems in many regions of the globe. In addition, the human influence on the environment contributes to a decline, in both quantity and quality, of the resources available for immediate consumption [**?**]. The agricultural and industrial practices conduct to higher pressure on natural resources and to many other environmental stresses (i.e., deforestation, increased water demand, pollution etc.,) [**? ? ?**].

Among the consequences of climate change, there are also health risks. An example of direct effect of the climate on health is the increased incidence of skin cancer [**?**] because of prolonged exposure to sunlight. However, most of the time the effects on health are mediated; such an example may be the increased contamination of groundwater with various pathogens because of higher frequency and intensity of floods. This results in enteric disease [**?**], often caused by the spread of pathogens like Campylobacter, Cryptosporidium, norovirus, or vibrio [**?**].

Climate change may extend the habitat of various parasites, like the liver fluke, which is a proven causal agent of cholangiocarcinoma, a highly aggressive form of liver cancer [**?**]. Equally dangerous, although insidious and more difficult to identify is the progressive salinization of groundwater in some inhabited areas close to sea, because of gradual sea levels rise, sometimes combined with changes in land use, like farming seawater animal species for human consumption. The higher content of salt in the drinking water has been connected with an increasing risk of arterial hypertension in the populations exposed [**? ?**].

Climate change influences the quality of the environment in numerous ways. Among these, a highly significant one is the mean air temperature, which influences the evapotranspiration of the hydrogeological basins, along with the land cover pattern. Starting from the beginning of this century, steady increases in the mean annual temperature were observed [**?**], and several models predict a continued rise in temperature during the 21st century [**? ? ? ? ? ?**]. The melting of glaciers represents a highly convincing proof of global warming [**? ? ? ? ? ?**].

Additionally, it was argued that the climate changes have a negative effect on groundwater recharge and ecosystems [**? ? ?**]. It was also found that the changes in land use impact on watersheds, surface water, land evapotranspiration, and groundwater [**?**]. Further, seawater intrusion due to the rising sea level, negatively influences the quality of the coastal fresh waters [**? ? ? ?**]. Thus, the climate change effect on the water resources is divided into quantity and quality impacts. Through the evapotranspiration and water availability, the quantity impact could be assessed as part of the water balance. In the specialty literature, there are numerous methods for the evapotranspiration calculation [**? ? ? ?**]. Incorporating the land cover, the crop evapotranspiration (ETc) is estimated using various methods such as Penman-Monteith method and 'New Implemented Spatial-Temporal On Regions–Climate Effect on Groundwater' (NISTOR-CEGW) [**? ?**].

The geological formations and the type of lithology play an important role in the aquifers typology, productivity of the aquifers, intrinsic vulnerability of the aquifers, and infiltration process. Thus, the effective precipitation becomes a significant parameter that is influenced by the climate and geology of the area. Because of these reasons, this work treats in detail both climate and territory aspects with respect to the water resources and risk assessment.

The development of various regions should take into account the current threats coming from changes in climate and in land use. In order to support the preservation of the environment and create a holistic image of the geographical region, the objectives of this work are focused to calculate the main parameters that influence the water resources in the Grand Est region and to integrate the geospatial data at 1 km^2 of these parameters for long-term periods of 1990s, 2020s, and 2050s. The product is important for the assessment of climate change effects on the water resources, groundwater vulnerability

determination, and future plans of water management. Through this study, the drought areas and high land use impact from the Grand Est region could be easily identified and used for advance analyses. The complexity of the survey is much consistent with integration of the terrain morphology and geology. This dataset is prepared for a risk assessment framework and it provides both spatial and temporal scales, especially for past, current, and mid 21st century.

2. Study Area

The Grand Est region is located in the northeastern part of France (Figure **??**) and it presents a variety of geological and geomorphological features, which are reflected by the morphology of the territory and water resources. The Vosges Mountains are located in the southeastern part of the Grand Est region and the Ardennes Mountains in the south-central and in northwest. The main rivers that cross the region are Rhine, Aube, and Marne [**?**]. Along these rivers are extending the largest valleys and lowlands of the region.

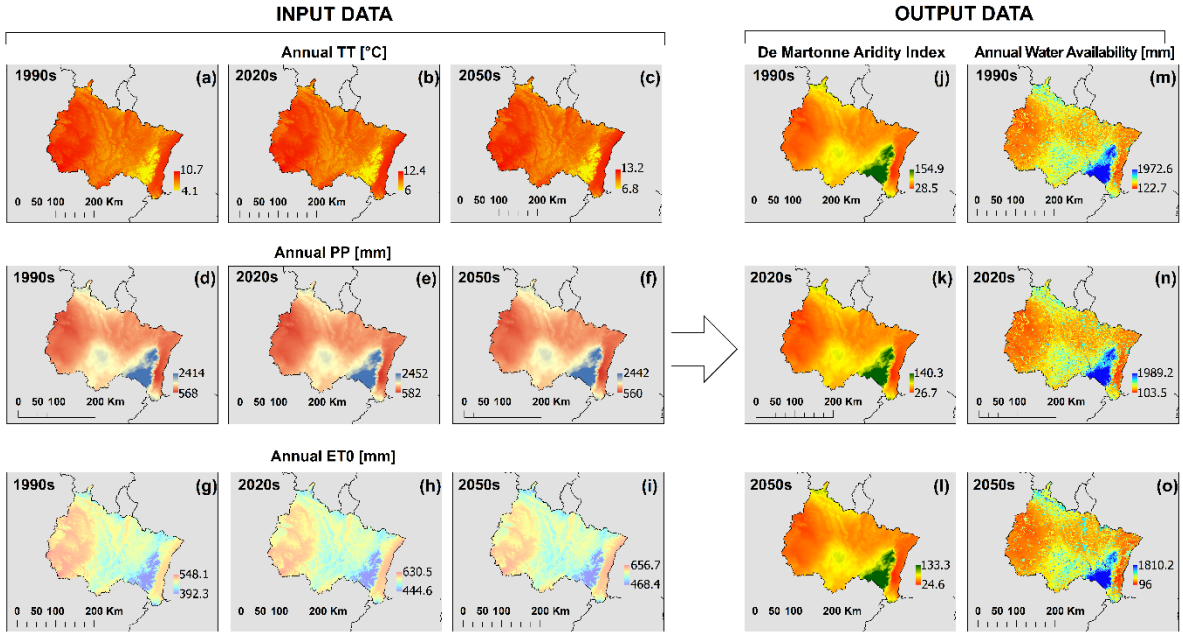

Figure 1. Climate variables as input data in the Grand Est region and output results. (**a**) Mean annual air temperature (TT) in 1990s. (**b**) Mean annual air temperature (TT) in 2020s. (**c**) Mean annual air temperature (TT) in 2050s. (**d**) Mean annual precipitation (PP) in 1990s. (**e**) Mean annual precipitation (PP) in 2020s. (**f**) Mean annual precipitation (PP) in 2050s. (**g**) Mean annual potential evapotranspiration (ET0) in 1990s. (**h**) Mean annual potential evapotranspiration (ET0) in 2020s. (**i**) Mean annual potential evapotranspiration (ET0) in 2050s. (**j**) De Martonne Aridity Index in 1990s. (**k**) De Martonne Aridity Index in 2020s. (**l**) De Martonne Aridity Index in 2050s. (**m**) Annual water availability in 1990s. (**n**) Annual water availability in 2020s. (**o**) Annual water availability in 2050s.

The geology of the Grand Est region presents a wide variety of formations. Thus, the chalkstones and limestones formations in the west and central parts, the dolomites are extended in the west-central, southern, and eastern parts, the jointed volcanic rocks, sandstones, and shales are present in the east, while the marls, clays, and sands are sparsely over the region and in the main valleys.

The region has a temperate climate with four seasons per year. The mean annual temperature ranges from 4 to 10 °C, while the precipitation regime exceeds 2000 mm/year in the Vosges Mountains [**?**]. The main climatic influence is coming from the Atlantic Ocean. According to the Koppen-Geiger climate classification, the region has a fully humid warm temperate climate with warm summers (Cfb class) [**?**].

The vegetation pattern is adapted to the relief and climate conditions of the region. The land use indicates large areas with agriculture cultivations in the eastern part, forest and natural grasslands in the center and western parts, while the main urban areas are located along the valleys, mainly in the eastern, central, northern, and western parts. The diversity of the land cover typology influences with different ranges the evapotranspiration and also the contamination of the phosphorus through pollution load of each land cover type.

3. Materials and Methods

3.1. Climate Data

The temporal frames used in this study for the climate data are 1961–1990 (for the 1990s), 2011–2040 (for the 2020s), and 2041–2070 (for the 2050s). The annual temperature, precipitation, and ET0 data were processed at high-spatial resolution (1 km^2). The main reason for the climate data analysis in such an investigation on water resources and risk is that the aridity-humidity status of the area is directly correlated with the water availability. In addition, the climate data and water availability variation in time over the Grand Est region is closely related to the assessment of risk of runoff leading to flooding, and the risk of infiltration, important for civil engineering projects and for predicting landslides and slope instability. Both aridity index—here De Martonne Aridity Index (Figure **??**j–l)—and water availability (Figure **??**m–o) were prepared at 1 km^2 resolution for the Grand Est region. Ref. [**?**] prepared the monthly climate models for Europe, from where we have extracted and processed the data for this study. He has used the Parameter Regression of Independent Slopes Model (PRISM) to compute the climate models of precipitation, while the ANUSplin interpolation method was used for the temperature models computation. A moderate climate change projection was applied, with emission of Representative Concentration Pathway (RCP) 4.5, which implies a global prediction of +1.4 °C (±0.5) [**? ?**]. The climate models of temperature and precipitation represent an ensemble average of 15 Atmosphere Ocean Global Climate Models (AOGCMs), which were processed according to the Coupled Model Intercomparison Project 5 (CMIP5) multi-model dataset, following the Intergovernmental Panel on Climate Change (IPCC) Assessment Report 5 [**?**]. The climate data models were performed into ClimateEU v4.63 environment, available on the website [**?**].

Previous works [**? ? ? ?**] described the data processing methods and the details on how the models were validated. Instead of bias corrections, a change factor (CF) method was applied to the raw GCM results. These climate models served as input for several studies and investigations at continental and regional scale [**? ? ?**].

3.2. Annual ETc and Annual AETc

The potential evapotranspiration (ET0) phenomena incorporating various patters of vegetation and land use is called crop evapotranspiration (ETc). In order to calculate the ETc, the ET0 in the study area was determined and a specific crop coefficient (Kc) was assigned to each land cover type. Thus, the annual ETc is calculated by multiplying the annual ET0 with the Kc (Equation (1)). For the annual ET0, the Thornthwaite formula [**?**] was used, while for the Kc values, the standard values were used [**?**]. This approach was previously used in several studies from the temperate zone [**? ?**]. The Kc values for the artificial and urban areas published by Ref. [**?**] were used in this work. **????** summaries the Kc values for with respect to the land cover of the Grand Est region.

Table 1. Corine land cover classes and appropriate annual Kc for present in the Grand Est region.

Corine Land Cover		Kc Annual				
CLC Code 2012	**CLC Description**	**Kc**	**Ks**	**Ku**	**Kw**	**Kclc**
111	Continuous urban fabric	-	-	0.3	-	0.29
112	Discontinuous urban fabric	-	-	0.2	-	0.21
121	Industrial or commercial units	-	-	0.3	-	0.3
122	Road and rail networks and associated land	-	-	0.3	-	0.25
123	Port areas	-	-	0.4	-	0.39
124	Airports	-	-	0.3	-	0.3
131	Mineral extraction sites	-	-	0.3	-	0.26
132	Dump sites	-	-	0.3	-	0.26
133	Construction sites	-	-	0.3	-	0.26
141	Green urban areas	-	-	0.2	-	0.21
142	Sport and leisure facilities	-	-	0.2	-	0.21
211	Non-irrigated arable land	1.14	-	-	-	1.14
212	Permanently irrigated land	1.25	-	-	-	1.25
213	Rice fields	0.94	-	-	-	0.94
221	Vineyards	0.5	-	-	-	0.5
222	Fruit trees and berry plantations	0.68	-	-	-	0.68
223	Olive groves	0.66	-	-	-	0.66
231	Pastures	0.7	-	-	-	0.7
241	Annual crops associated with permanent crops	0.67	-	-	-	0.67
242	Complex cultivation patterns	1.16	-	-	-	1.16
243	Land principally occupied by agriculture, with significant areas of natural vegetation	0.92	-	-	-	0.92
244	Agro-forestry areas	0.92	-	-	-	0.92
311	Broad-leaved forest	1.42	-	-	-	1.42
312	Coniferous forest	1	-	-	-	1
313	Mixed forest	1.33	-	-	-	1.33
321	Natural grasslands	0.97	-	-	-	0.97
322	Moors and heathland	0.92	-	-	-	0.92
323	Sclerophyllous vegetation	0.62	-	-	-	0.62
324	Transitional woodland-shrub	0.83	-	-	-	0.83
331	Beaches, dunes, sands	-	0.23	-	-	0.23
332	Bare rocks	-	0.15	-	-	0.15
333	Sparsely vegetated areas	0.48	-	-	-	0.48
334	Burnt area	-	0.1	-	-	0.1
335	Glaciers and perpetual snow	-	-	-	0.51	0.51
411	Inland marshes	-	-	-	0.45	0.45
412	Peat bogs	-	-	-	0.37	0.37
421	Salt marshes	-	-	-	0.32	0.32
422	Salines	-	0.1	-	-	0.1
423	Intertidal flats	-	-	-	0.64	0.64
511	Water courses	-	-	-	0.63	0.63
512	Water bodies	-	-	-	0.64	0.64
521	Coastal lagoons	-	-	-	0.68	0.68
522	Estuaries	-	-	-	0.62	0.62
523	Sea and ocean	-	-	-	0.74	0.74

Kc—crop coefficient for plants, Ks—evaporation coefficient for bare soils, Ku—crop coefficient for urban areas, Kw—evaporation coefficient for open water, Kclc—crop coefficient for land cover. Source: [**? ?**]

Table 2. Corine land cover classes and calculated annual Kc for future scenarios in the Grand Est region.

Corine Land Cover			Kc				
CLC Code 2012	**CLC Projection Code**	**CLC Description**	**Kc**	**Ks**	**Ku**	**Kw**	**Kclc**
133	0	Built-up area	-	-	0.26	-	0.26
211	1	Arable land (non-irrigated)	1.14	-	-	-	1.14
231	2	Pasture	0.7	-	-	-	0.7
321 and 324	3	Natural and semi-natural vegetation (including Natural grasslands, scrublands, regenerating forest below 2 m, and small forest patches within agricultural landscapes)	0.9	-	-	-	0.9
411	4	Inland wetlands	-	-	-	0.45	0.45
335	5	Glaciers and snow	-	-	-	0.51	0.51
212	6	Irrigated arable land	1.25	-	-	-	1.25
321	7	Recently abandoned arable land (i.e., "long fallow"; includes very extensive farmland not reported in agricultural statistics, herbaceous vegetation, grasses and shrubs below 30 cm)	0.97	-	-	-	0.97
241	8	Permanent crops	0.67	-	-	-	0.67
313	10	Forest	1.33	-	-	-	1.33
333	11	Sparsely vegetated areas	0.48	-	-	-	0.48
331	12	Beaches, dunes and sands	-	0.23	-	-	0.23
422	13	Salines	-	0.1	-	-	0.1
423 and 521	14	Water and coastal flats	-	-	-	0.66	0.66
322	15	Heathland and moorlands	0.92	-	-	-	0.92
231 and 324	16	Recently abandoned pasture land (includes very extensive pasture land not reported in agricultural statistics, grasses and shrubs below 30 cm)	0.76	-	-	-	0.76

Kc—crop coefficient for plants, Ks—evaporation coefficient for bare soils, Ku—crop coefficient for urban areas, Kw—evaporation coefficient for open water, Kclc—crop coefficient for land cover. Source: [**? ?**]

The annual actual crop evapotranspiration (AETc) is the closer estimation of the real ETc, that incorporates in the calculation the annual precipitation and aridity index. For the AETc determination, the Budyko approach [**?**] was used because of its applicability on long-term period and large area. The Budyko formula (Equation (2)) is a useful method for the hydrological studies and water balance calculation because of the consideration of heat energy and precipitation which are taken into account [**?**]. Recently, numerous studies based on the Budyko equation indicate good performance [**? ?**]. The mathematical operations between raster layers were completed using ArcGIS environment.

$$\text{Annual ETc} = \text{annual ET0} \times \text{annual Kc} \quad (1)$$

$$\frac{\text{AETc}}{\text{PP}} = \left[\left(\varphi tan\frac{1}{\varphi}\right)(1 - exp^{-\varphi})\right]^{0.5} \quad (2)$$

where:

AET cactual land cover evapotranspiration (mm)
PP total annual precipitation (mm)
Φ aridity index (Equation (3))

$$\Phi = \text{ETc/PP} \quad (3)$$

3.3. Geological Data and Aquifers

Jointed and karstified rocks such as limestones, chalkstones, sandstones, and conglomerates, are representative for the geology of the Grand Est region. In addition, volcanic and plutonic rocks, and also gneisses, marls, clays, shales, mica schists, quartzites, and gravels could be found in the study area. The lithological layers (Figure **??**a), together with the relief morphology, control the water flow direction and infiltration rate into the soil. This amount of infiltration is important also for the aquifers' recharge and the soil water content [**?**]. Thus, the typology of rocks plays a significant role in

determining aquifers types, permeability, saturation of the soil, and infiltration process [**? ?**]. The last two processes could take varied time and are dependent on lithology and rainfall intensity.

According to the geology, six types of productivity aquifers were defined in the International Hydrogeological Map of Europe, dating from 2013, at 1:1,500,000 scale [**?**]. The aquifer types include fractured and porous media, and also rocks which are not considered aquifers. The main aquifers types, identified in the International Hydrogeological Map of Europe according to the productivity type are: highly productive fissured aquifers, highly productive porous aquifers, low and moderately productive fissured aquifers, low and moderately productive porous aquifers, locally aquiferous rocks—porous or fissured, and practically non-aquiferous—porous or fissured (Figure **??**b).

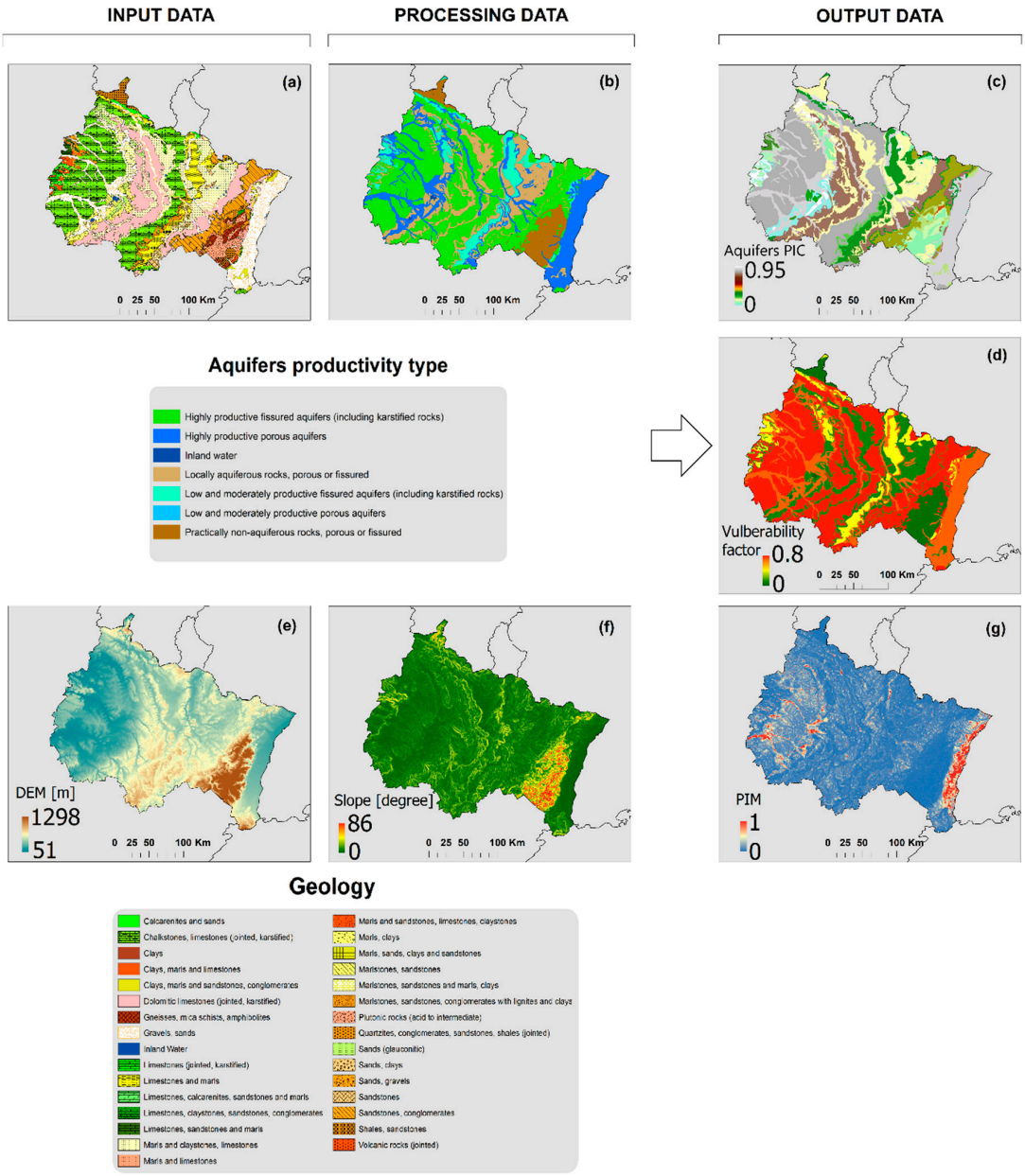

Figure 2. Grand framework of geological and terrain data, processing, and results from these layers the Grand Est region. (**a**) Geological formations map. (**b**) Aquifers productivity type map. (**c**) Potential infiltration coefficient (PIC) map. (**d**) Hydrogeological vulnerability factor (HVF) map. (**e**) Digital elevation model (DEM) map. (**f**) Slope angle map. (**g**) Potential infiltration map (PIM). Note: Potential infiltration map was calculated as the ratio of potential infiltration coefficient and normalization slope layer (radian degrees).

3.4. Terrain Data and Potential Infiltration Map

The digital elevation model (DEM) of the Grand Est region was used for the slope angle and potential infiltration map calculation. The Rhine Valley in the eastern part and the Marne and Aube Valleys in the western part represent the lowlands in the Grand Est region. The highest elevations are recorded in the south-east side of the region, where the Vosges Mountains are present. The altitudes in the study area vary from 51 m to 1298 m above sea level (Figure **??**e), thus the relief morphology influences greatly the runoff flow. By combining relief morphology and lithology, the groundwater flow directions and accumulation could be estimated at spatial scale.

The DEM layer is important in water resources and environmental risks studies, not only because of the influence of variations of relief topography and slopes' angle gradient on the water flow direction and infiltration control, but also because of their role in flooding, flow accumulation, and slope stability. With that in mind, using the slope angle layer (Figure **??**f) together with the PIC layer, which reflects the lithology permeability, a potential infiltration map (PIM) was drawn (Figure **??**g). The calculation is based on the reasoning that where the PIC is higher and the slope angle is lower, the infiltration values will be higher. This approach was developed using the ratio between PIC and slope angle (normalized values). The procedure was also applied before in studies of groundwater [**? ?**]. ArcGIS environment served as the software to analyze and manage the data assignation of aquifers' features in the attribute table.

3.5. Land Cover Data and Pollution Load Index

The land cover has a two-fold significance for water resources and environmental risk mapping. First, the quantitative aspect is related to the evapotranspiration, which determines the final water availability amount. Second, the qualitative aspect includes the pollution load because of phosphorus transfers, corresponding to each type of land cover. For these two aspects, the spatial distribution of crop coefficient (Kc) and pollution load index (PLI) [**?**] in different periods over the Grand Est region, were determined by using the CORINE Land Cover database and Hercules projections. The CORINE Land Cover database data used were from 1990 to 2012, the source being Copernicus Land Monitoring Services [**?**]. The Hercules projections indicate four land cover models related to 2040. These future projections were developed within the framework of "Sustainable futures for Europe's HERitage in CULtural landscapES" (HERCULES) project [**?**]. The methodology applied in this project is based on the macro-economic and land use models, following fourteen trajectories in the land cover changes trend [**?**].

3.6. Effective Precipitation

The effective precipitation represents the amount of water that infiltrates and contributes to the groundwater recharge. For the calculation of effective precipitation, the water availability and potential infiltration map were considered at spatial scale of the Grand Est region (Figure **??**a–f). The precipitation, lithology permeability, soil saturation, and terrain configuration are the main drivers for the infiltration process. For this reason, all these factors were used for effective precipitation by adopting the formula from equation (Equation (4)). Being a study for a long-term period (averages of 30 years), the storage yield was neglected.

$$EP = WA \times PIM \quad (4)$$

where:

EP, Effective precipitation (mm)
WA, Water availability (mm)
PIM, Potential infiltration map (dimensionless)

The calculations were completed at spatial scale using ArcGIS environment and the normalized raster of PIM, following the normalization procedure [**?**]. The procedures of the calculation with respect to the surface and subsurface hydrologic properties, soil infiltration capacity, lithology, slope, and land use implication for the effective precipitation are in line with the previous studies [**? ?**].

3.7. Normalization of Data

In order to obtain a homogeneous database, all datasets were normalized between 0 and 1. Thus, the effective precipitation (EF, for 1990s, 2020s, and four scenarios for 2050s), the pollution load index (PLI) (CLC1990, CLC2012, and HERCULES Projections 2040), the potential infiltration coefficient (PIC), the hydrogeological vulnerability factor (HVF), and the potential infiltration map (PIM) were normalized and processed in a unique scale. Data normalization was done in conformity with the standard formula (Equation (5)). In this way, the datasets are ready for risk mapping analysis and other various spatial interference.

$$Xnorm = (X - Xmin)/(Xmax - Xmin) \quad (5)$$

where,

X, the values in series
Xnorm, the value after normalization
Xmax, the maximum value sin the series
Xmin, the minim value in the series

The data presented in this work were validated through publications [**? ?**] regarding the climate change effect on groundwater resources in the Grand Est region, but also through spatial analysis in ArcGIS regarding the groundwater vulnerability [**?**].

4. Results

4.1. Variation of Climate Parameters

4.1.1. Climate Models of Temperature and Precipitation

The climatological maps indicate a mean annual air temperature from 4.1 °C to 10 °C (Figure **??**a) (1990s), but with predicted increases up to 12.4 °C (2020s) and 13.2 °C (2050s) (Figure **??**b,c). During the 1990s, the annual precipitation values range was from 568 mm to 2414 mm (Figure **??**d). The higher temperatures are in the western and eastern parts of the region, mainly in the lowlands and valleys. The low temperatures were identified in the Vosges Mountains and central parts of the region. The climate models indicate annual precipitation values between 582 mm and 2452 mm during the 2020s and between 560 mm and 2442 mm in the 2050s (Figure **??**e,f). The higher amount of precipitation is depicted in the Vosges Mountains and in the South-central part of the Grand Est region. The potential evapotranspiration (ET0) varied in the study area from 392 mm to 548 mm in the past period (1990s) (Figure **??**g), while the current period (2020s) indicates values from 444 mm to 630 mm (Figure **??**h). During the 2050s, the ET0 predicted values ranging from 468 mm to 656 mm (Figure **??**i). The higher values of ET0 were identified in the western and eastern parts, while the lower values of ET0 were found in the Vosges Mountains.

4.1.2. Variation of the De Martonne Aridity Index

The spatial variation of the De Martonne Aridity Index in the Grand Est region during 1990s indicates extremely humid climate (index higher than 55) in the Vosges Mountains. The very humid (values from 35 to 55) and humid (values above 28 and below 35) climates were found in major parts of the territory (Figure **??**j). In 2020s and 2050s, the climate will be semi-humid in some locations from east and west of the Grand East region, with lower values (below 28) of the De Martonne Aridity Index

(Figure **??**k–l). This means that during the 2020s and 2050s, the De Martonne Aridity Index decreases and indicates gradual aridization. In the future periods, the very humid and extremely humid climates are depicted in the mountain areas and in the central parts of the Grand Est region.

4.1.3. Variation of Water Availability and Evapotranspiration

The spatial distribution of water availability during the 1990s period in the Grand Est region shows values between 122 mm and 1972 mm. The higher values (above 1000 mm) were depicted in the south-central, south-eastern, and north-western areas (Figure **??**m). The lower values (below 300 mm) of water availability were identified in the western and eastern parts, especially in the Marne Valley, Aube Valley, and Rhine Valley. In 2020s and 2050s, the water availability ranges from 103 mm to 1989 mm and from 96 mm to 1810 mm (Figure **??**n–o). In the future periods, the high water availability values are extended in the Vosges Mountains while the low values are located in the Rhine, Marne and Aube Valleys.

Combining the climate models and land cover data, the annual ETc and AETc were calculated at spatial scale of the Grand Est region. During the 1990s, the annual ETc varied from 92 mm to 777 mm (Figure **??**a). The higher values were depicted in the western, eastern, and central parts of the region, while the lower values were found in the mountains and urban areas. In the period of 2020s, the annual ETc indicates values between 102 mm and 892 mm (Figure **??**b). The future scenarios of the 2050s period show values between 138 mm and 873 mm of the ETc (Figure **??**c–f). The future scenario has almost the same pattern, with few modifications that follow the land cover projections.

The spatial distribution of the annual AETc indicates values from 92 mm to 650 mm during 1990s, with high values in the central and south-eastern parts of the region (Figure **??**g). The lower values of the AETc were found in the west and east, and also in the urban areas. In the 2020s, the annual AETc shows values between 100 mm and 737 mm (Figure **??**j). The projections for 2050s show values between 136 mm and 723 mm. It is interesting that the AETc increases the values for the 2050s in the mountains area. For the future periods, the lower values of AETc were depicted in the valleys, where the annual precipitation is low.

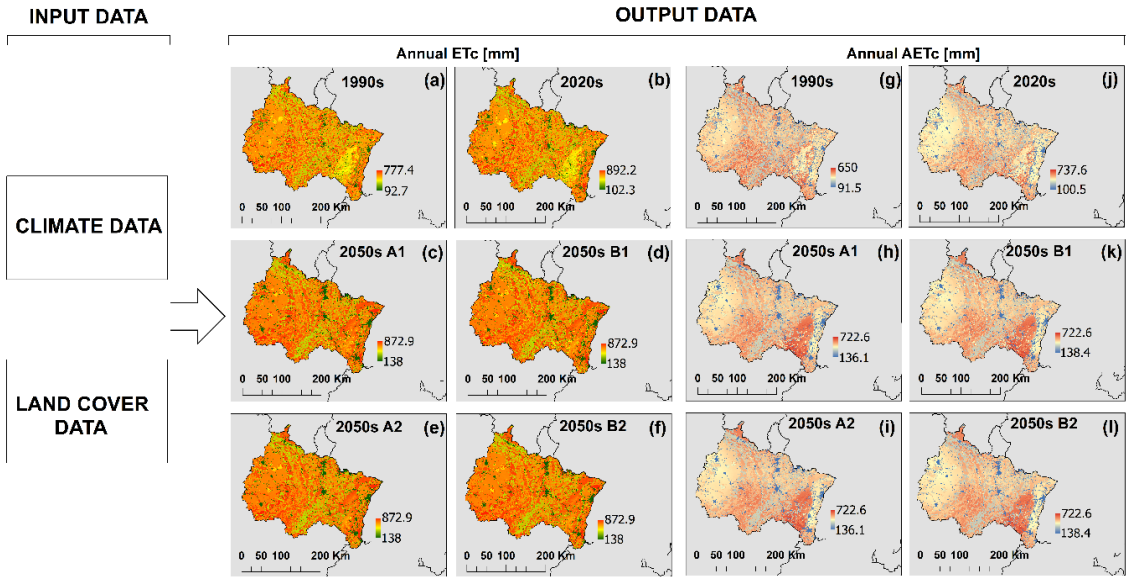

Figure 3. Spatial distribution of annual crop evapotranspiration (ETc) and annual actual crop evapotranspiration (AETc) in the Grand Est region. (**a**) ETc in 1990s. (**b**) ETc in 2050s, Scenario A1. (**c**) ETc in 2050s, Scenario A2. (**d**) ETc in 2020s. (**e**) ETc in 2050s, Scenario B1. (**f**) ETc in 2050s, Scenario B2. (**g**) AETc in 1990s. (**h**) AETc in 2050s, Scenario A1. (**i**) AETc in 2050s, Scenario A2. (**j**) AETc in 2020s. (**k**) AETc in 2050s, Scenario B1. (**l**) AETc in 2050s, Scenario B2.

4.2. Variation of Kc and PLI

In the Grand Est region, the land cover pattern is complex, with a multitude of vegetation type and artificial areas. The broad-leaved, coniferous, and mixed forests are located predominantly in the mountains and hilly areas. The arable and croplands extend in the lowlands and the main valleys of Rhine, Aube, and Marne. The cities and villages are spread over the region, and their areas are expected to increase by the mid-21 century. Each land cover type has a particular capacity for evapotranspiration [**?**]. Specific annual Kc values (**????**) for each type of vegetation and land use were assigned to the land cover layer. The method follows the Ref. [Haidu and Nistor and Mindrescu] approach and this procedure contributes to the annual ETc and AETc. Figure **??**a–f shows the spatial variation of the Kc over the Grand Est region. The higher values were depicted in the agriculture and forest areas, while the lower values overlap with the industrial units, road and rail networks, and construction sites.

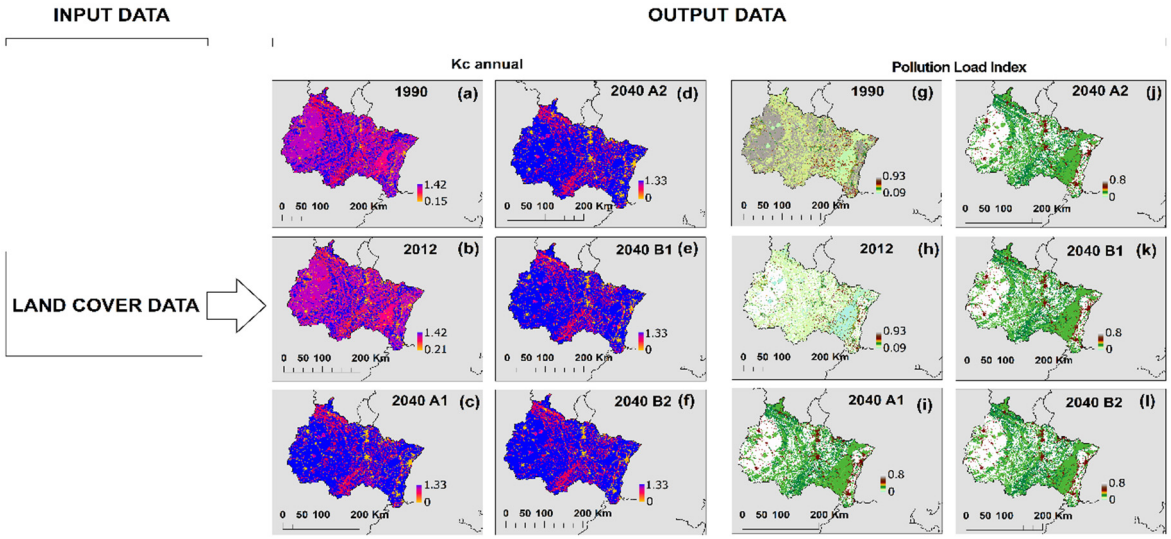

Figure 4. Spatial distribution of crop coefficient (Kc) and pollution load index (PLI) in the Grand Est region. (**a**) Kc in 1990s. (**b**) Kc in 2012. (**c**) Kc in 2040, Scenario A1. (**d**) Kc in 2040, Scenario A2. (**e**) Kc in 2040, Scenario B1. (**f**) Kc in 2040, Scenario B2. (**g**) PLI in 1990s. (**h**) PLI in 2012. (**i**) PLI in 2040, Scenario A1. (**j**) PLI in 2040, Scenario A2. (**k**) PLI in 2040, Scenario B1. (**l**) PLI in 2040, Scenario B2.

Regarding the quality of the environment relative to land cover, the literature [**? ?**] proposed a particular PLI for each land cover type. Thus, we assigned the specific PLI for each land cover type in the ArcGIS environment. Figure **??**g–l indicates the spatial variation of pollution load index in the study area. These results are highly recommended for use in the spatial analysis of water resources and other environmental risks evaluation. In the Grand Est region, the PLI has higher values in the agricultural areas, mainly in the Rhine, Marne, and Aube Valleys. The low values of PLI are associated with the pastures, sparsely vegetated areas, bare rocks, peat bogs, salt marshes, and water courses.

The values of the PLI used in the present study are reported in the **????**.

Table 3. Corine land cover classes and relative pollution load index applied for the 2012 in the Grand Est region.

CLC Code 2012	CLC Description	Pollution Load Index	Normalized Vulnerability Coefficient
111	Continuous urban fabric	6	0.40
112	Discontinuous urban fabric	5.5	0.36
121	Industrial or commercial units	5	0.33
122	Road and rail networks and associated land	7.5	0.50
123	Port areas	7	0.46
124	Airports	7	0.46
131	Mineral extraction sites	9	0.60
132	Dump sites	14	0.93
133	Construction sites	7	0.46
141	Green urban areas	3.5	0.23
142	Sport and leisure facilities	4	0.26
211	Non-irrigated arable land	12	0.80
212	Permanently irrigated land	15	1.00
213	Rice fields	13.5	0.90
221	Vineyards	6	0.40
222	Fruit trees and berry plantations	5	0.33
223	Olive groves	4.5	0.30
231	Pastures	3.5	0.23
241	Annual crops associated with permanent crops	9	0.60
242	Complex cultivation patterns	8.3	0.55
243	Land principally occupied by agriculture, with significant areas of natural vegetation	5.5	0.36
244	Agro-forestry areas	3	0.19
311	Broad-leaved forest	3.6	0.23
312	Coniferous forest	2.5	0.16
313	Mixed forest	2.8	0.18
321	Natural grasslands	2.5	0.16
322	Moors and heathland	2.7	0.17
323	Sclerophyllous vegetation	2.5	0.16
324	Transitional woodland-shrub	2.6	0.17
331	Beaches, dunes, sands	2.5	0.16
332	Bare rocks	1.5	0.09
333	Sparsely vegetated areas	2	0.13
334	Burnt area	5	0.33
335	Glaciers and perpetual snow	0.1	0.007
411	Inland marshes	2.3	0.15
412	Peat bogs	2.3	0.15
421	Salt marshes	2.3	0.15
422	Salines	2.3	0.15
423	Intertidal flats	3	0.19
511	Water courses	3	0.19
512	Water bodies	3	0.19
521	Coastal lagoons	3	0.19
522	Estuaries	3	0.19
523	Sea and ocean	3	0.19

Source: Ref. [**?**]

Table 4. Corine land cover classes and relative pollution load index applied for the future scenarios (2040s) in the Grand Est region.

CLC Code 2012	CLC Projection Code	CLC Description	Pollution Load Index	Normalized Vulnerability Coefficient
133	0	Built-up area	7	0.46
211	1	Arable land (non-irrigated)	12	0.8
231	2	Pasture	3.5	0.23
324	3	Natural and semi-natural vegetation (including Natural grasslands, scrublands, regenerating forest below 2 m, and small forest patches within agricultural landscapes)	2.6	0.17
411	4	Inland wetlands	2.3	0.15
335	5	Glaciers and snow	0.1	0
212	6	Irrigated arable land	15	1
321	7	Recently abandoned arable land (i.e., "long fallow"; includes very extensive farmland not reported in agricultural statistics, herbaceous vegetation, grasses and shrubs below 30 cm)	2.5	0.16
241	8	Permanent crops	9	0.6
313	10	Forest	2.8	0.18
333	11	Sparsely vegetated areas	2	0.13
331	12	Beaches, dunes and sands	2.5	0.16
422	13	Salines	2.3	0.15
521	14	Water and coastal flats	3	0.19
322	15	Heathland and moorlands	2.7	0.17
324	16	Recently abandoned pasture land (includes very extensive pasture land not reported in agricultural statistics, grasses and shrubs below 30 cm)	2.6	0.17

Source: Ref. [**? ?**].

4.3. Variation of PIC, HVF, and PIM

The PIC and HVF values are related to the geological formations and lithology, while the PIM is related to the geology and terrain morphology. Thus, based on the geological data and type of aquifers, the most important outputs, consisting in the potential infiltration coefficient (PIC) [**? ?**] and in aquifers' vulnerability factor were assigned [**?**] to the aquifers layer. In the Grand East region, the higher value of PIC are located in the areas with gravels, sands, limestones, and dolomitic formations. The lower values of PIC are mainly identified in the areas with clays and marls. The determination of PIC (Figure **??**c) at spatial scale plays a crucial role in the effective infiltration calculation [**?**].

The HVF layer (Figure **??**d) is significant for the groundwater vulnerability mapping [**?**]. In the last years, the specialists in hydrogeology and environmental studies have used successfully the PIC and vulnerability factors in European aquifers into CC-WARE European Project [**?**] and DRINK Adria Project [**?**]. Table **??** reports the aquifer vulnerability factors used in the Grand Est region. The higher values of HVF are found in the dolomitic, limestones, calcarenites, and sands. The lower HVF is related to the areas with marls, clays, gneiss, mica, schists, plutonic rocks, shales, and claystones.

The PIM of the Grand Est region was generated using the DEM, slope angle, and PIC layers. High values of the PIM were depicted in the lowlands, mainly in the valleys with gravels and sands deposits. These areas show higher infiltration values because of higher PIC and low slope angle. As we can observe in Figure **??**g, the areas with high values of PIM overlap with the Rhine, Marne, and Aube Valleys. The major part of the Grand Est territory appears with low infiltration rate, because of the low PIC values and multitude of slopes. Vosges Mountains, where the plutonic rocks are, represent a territory with an impermeable lithology layer.

Table 5. Aquifers productivity in Grand Est region.

Aquifers Type	Vulnerability Factor
Highly productive fissured aquifers (including karstified rocks)	0.8
Low and moderately productive fissured aquifers (including karstified rocks)	0.4
Highly productive porous aquifers	0.7
Low and moderately productive porous aquifers	0.3
Locally aquiferous rocks, porous or fissured	0.1
Practically non-aquiferous rocks, porous or fissured	0.05
Snow field/ice field	0

Source: Ref. [**?** **?**].

4.4. Variation of Effective Precipitation

One of the most complex layers from the calculation point of view and with major importance for the water resources and groundwater vulnerability assessment is the effective precipitation layer. In the Grand Est region, the effective precipitation varied from 0 mm to 636 mm (1990s and 2020s). The high values were found in the Rhine Valley and along main rivers banks (Figure **??**a). The lower values of effective precipitation could be depicted in major parts of the territory. During the 2050s, the effective precipitation ranges from 0 mm to about 572 mm. The higher values of the effective precipitation were found in the large valleys, but with less amount of this parameter. The significant changes between past and future could be observed in the central and north-central parts (Figure **??**c–f). The Vosges Mountains record low values of the effective precipitation both for past and future periods. Few territories from north and north-west appear with high effective precipitation values (over 500 mm). The results of the low effective precipitation are influenced by the PIC (below 0.2), mainly in the mountain areas of Vosges and Ardennes Mountains, where the non-aquiferous rocks were defined (BGR and UNESCO, 2013). On the other hand, the areas with higher PIC (above 0.8), the composition of the aquifers, mainly composed of gravels, sands, and limestones, are affected by climate change because of low values of water availability.

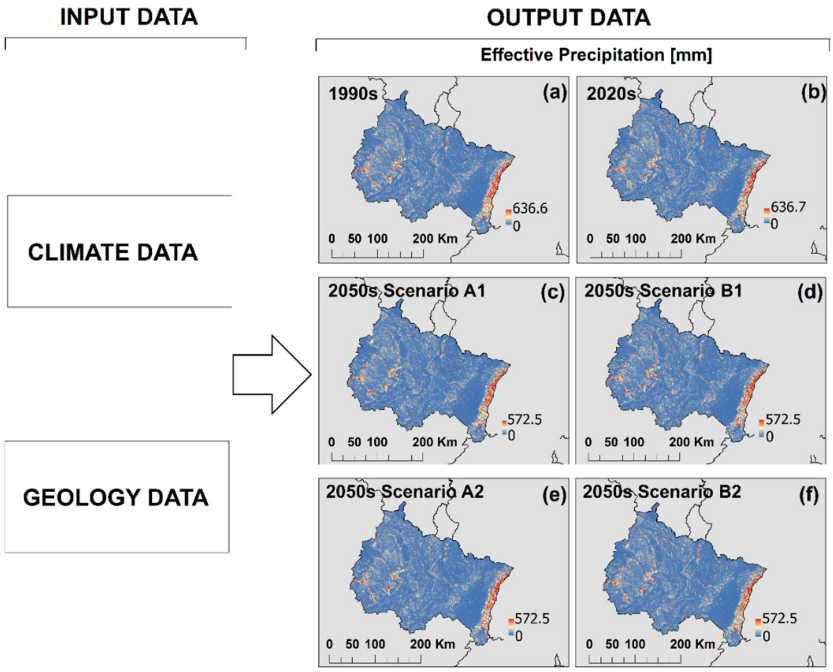

Figure 5. Spatial distribution of effective precipitation in the Grand Est region. (**a**) Effective precipitation in 1990s. (**b**) Effective precipitation in 2020s. (**c**) Effective precipitation in 2050s, Scenario A1. (**d**) Effective precipitation in 2050s, Scenario B1. (**e**) Effective precipitation in 2050s, Scenario A2. (**f**) Effective precipitation in 2050s, Scenario B2.

4.5. Normalized Layers

Figure **??** shows the normalized maps of effective precipitation, PLI, PIC, HVF, and PIM in the Grand Est region, France. These maps represent a comprehensive gridded dataset that serves for the climate and pollution risk evaluation in the study area with respect to the water resources. The data grids are homogenous layers ready for different kind of analyses, such as spatial analysis by weights, inference matrix, fuzzy logic, or any other approach that is focused on the quality and quantity assessment of nowadays and future factors. In addition, our database includes the future scenarios for the 2020s and 2050s, that could help for the environmental planning and delineation of protection zones.

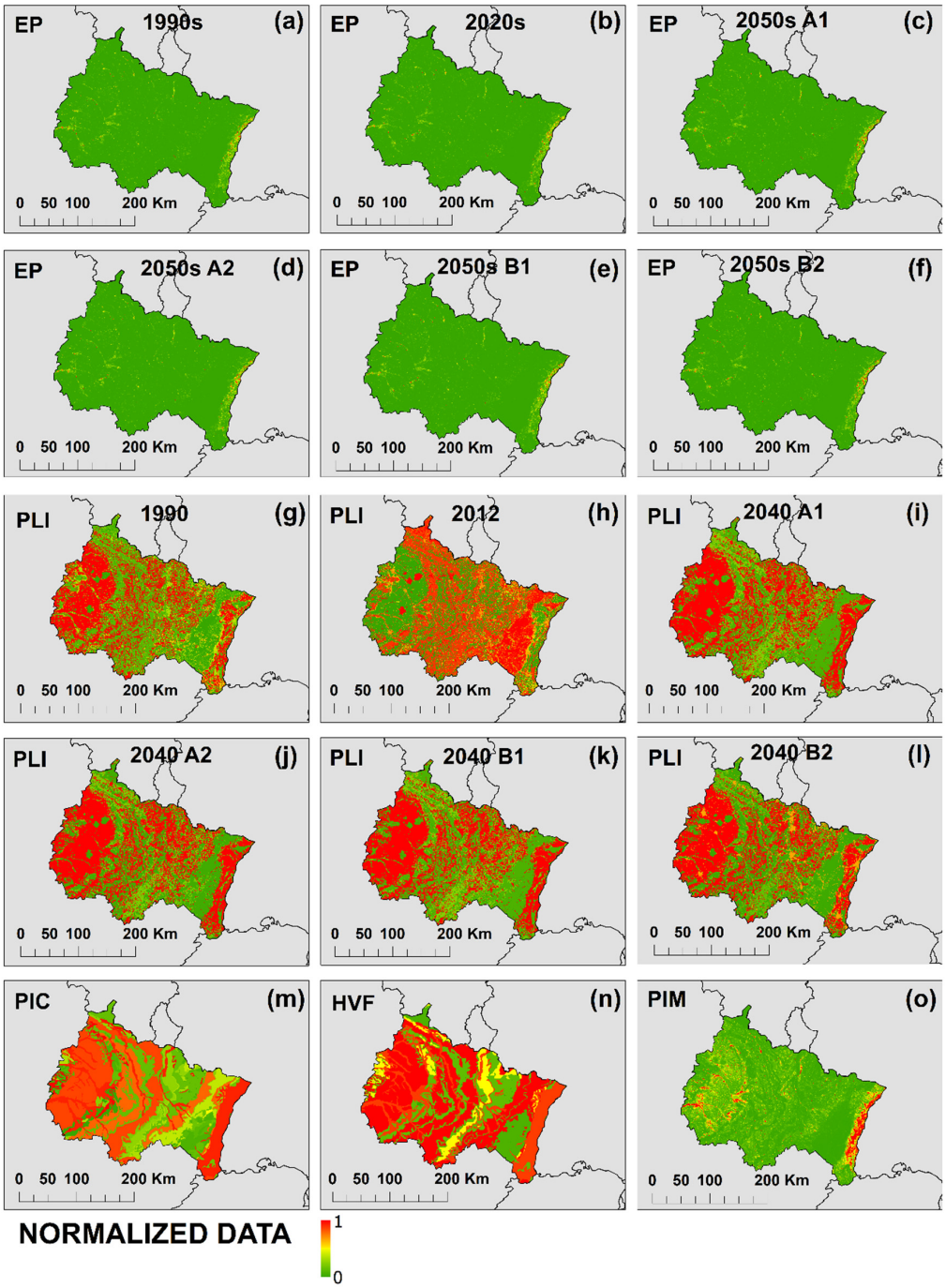

Figure 6. Normalization layers of effective precipitation (EP) (**a**–**f**), pollution load index (PLI) (**g**–**l**), potential infiltration coefficient (PIC) (**m**), hydrogeological vulnerability factor (HVF) (**n**), and potential infiltration map (PIM) (**o**) in the Grand Est region.

5. Discussion on the Usage Notes

The comprehensive gridded dataset based on GIS technology and complex approaches was set-up for the Grand Est region, France. The gridded dataset is associated with the climate models, geology, terrain morphology, and land cover and it represents a useful cartographical support for water resources analysis and environmental risk evaluation in the Grand Est region of France. The uniform representation of climate data, geological and aquifers data, terrain and potential infiltration map data, effective precipitation, land cover data and pollution load index, as well as annual crop

evapotranspiration and annual actual crop evapotranspiration were combined and described using a regular grid cell of 1 km^2.

The results indicate a negative impact of climate change on the water resources for the future periods. Analyzing the De Martonne Aridity Index variation, the index decreased during the 2020s and 2050s. This fact clearly indicates slight aridization and it suggests the negative effect of climate change in the region. The annual ETc and AETc values increase for the future, while the water availability decreases for the 2050s.

The land cover pattern indicates a large variety in the Grand Est region. Thus, the values of Kc and PLI show a wide range starting from the artificial areas, to the agriculture, pasture, and forest. For this reason, the importance of the land cover for the water resources has two-fold impact: a quantitative one, in terms of evapotranspiration and water availability amount, and a qualitative one, related to the phosphorous and load pollution variation in different kinds of land cover.

The PIC, HVF, and PIM are essential layers with respect to the substrate data and infiltration process. Thus, these three layers are useful for the aquifers recharge and groundwater vulnerability calculation.

The effective precipitation layer illustrates directly the areas with high amounts of water that infiltrate in the fractured and porous media. Considering that the geological formations do not change in a temporal scale of 100 years, the decline of the effective precipitation in the Grand Est region is due to climate change.

The originality of this study consists in providing the first regional high-resolution datasets on various patterns of distribution of the variables studied, over the Grand Est region. The work and layers prepared here are essential for water resources management and future predictions, but could be also useful for different environmental hazards, such as flooding, landslides, or droughts. These layers are appropriate files for development of the groundwater vulnerability map using spatial analyst tools in ArcGIS, on one hand, but also for the flow accumulation and flood areas determination, on other hand. This comprehensive dataset of the Grand Est region can be combined with additional datasets (e.g., groundwater table, soil properties) and used as a driver for hazard maps in the region. In this sense, TRIGRS and Scoops 3D are highly used for slope stability because of the large GIS data reading and results at spatial scale. Thus, the work presented here completes the previous studies of the Grand Est region, offering a much more complex homogenous dataset. An example may be provided by the spatial analysis, using GIS technology for groundwater vulnerability mapping, over the Grand Est region, performed by Ref. [**?**].

To support the development of climate change mitigation planning for water and natural resource management in the Grand Est region, and also in the scientific community, we provide the gridded data layers through the zenodo platform [**?**].

6. Conclusions

In this work, the main layers of temperature, precipitation, geology, terrain configuration, and land cover of the Grand Est region were used to analyze the annual ETc, AETc, water availability, PIC, HVF, PIM, and effective precipitation. In order to serve as a comprehensive gridded dataset for the climate change and water resources risk assessment, all these layers were processed at 1 km^2 spatial resolution and normalized. The strength of comprehensive gridded dataset processed in this study lies in the future datasets, which are of high interest for both the scientific community and the administrative authorities of the region. This region represents a study case of the relationship between climate change and agriculture. Our comprehensive gridded dataset provides the "stand alone" maps and derived maps, as well as the normalization of all layers.

The findings presented in this paper illustrate the decreasing of the De Martonne Aridity Index, which suggests negative impact of climate change on the Grand Est territory through the aridization. The annual ETc and AETc increase and the water availability and effective precipitation decrease for the future periods in the study area. The high values of the water availability could be identified in the Vosges and Ardennes Mountains, where the annual precipitation amount is higher than

the evapotranspiration. On the contrary, in the mountain areas, the lithological strata are much impermeable and the infiltration is very low. For this reason, the HVF is very low in the area of Vosges and Ardennes Mountains.

The pollution load index (PLI) indicates higher values in the agricultural areas, more precise in the Rhine, Marne, and Aube Valleys and it has lower values in the natural areas such pastures and vegetated areas, bare rocks, marshes, and water courses.

Thus, the environmental planning for the near future and mid-century time period could consider the original maps that we have developed in this work. Moreover, the comprehensive gridded dataset contributes to environmental risk evaluation and to the calibration of various models (e.g., groundwater flow models, slope stability analyses). The technical validation of the presented data and methodology is supported by the previous publications [**? ?**], while future work may develop a more extensive dataset including hydrological models based on runoff and groundwater flow, spring discharge monitoring, and field research data including soil sampling and geotechnical investigations.

Author Contributions: M.-M.N. conducted the analysis and wrote the Abstract and Note Usage sections. He performed the figures and tables. I.H. wrote the Methods section. Ş.D. wrote the Technical Validation section. C.Ş. wrote the Introduction section, completed the whole research, and wrote the paper. All authors have read and agreed to the published version of the manuscript.

Funding: This research received no external funding.

Acknowledgments: The authors would like to thank Andreas Hamann for the climate data models. No grant was used to carry out this work, considering that these are the data descriptors of the previous studies of the authors.

Conflicts of Interest: The authors declare no conflict of interest for this paper.

References

1. Islam, M.A.; Hoque, M.A.; Ahmed, K.M.; Butler, A.P. Impact of climate change and land use on groundwater salinization in southern Bangladesh—Implications for other Asian deltas. *Environ. Manag.* **2019**, *64*, 640–649. [CrossRef] [PubMed]
2. Scheelbeek, P.F.; Chowdhury, M.A.; Haines, A.; Alam, D.S.; Hoque, M.A.; Butler, A.P.; Khan, A.E.; Mojumder, S.K.; Blangiardo, M.A.; Elliott, P.; et al. Drinking water salinity and raised blood pressure: Evidence from a cohort study in coastal Bangladesh. *Environ. Health Perspect.* **2017**, *125*, 57007. [CrossRef] [PubMed]
3. IPCC. Climate change 2001: The scientific basis. In *Contribution of Working Group I to the Third Assessment Report of the Intergovernmental Panel on Climate Change*; Houghton, J.T., Ding, Y., Griggs, D.J., Noguer, M., van der Linden, P.J., Dai, X., Eds.; Cambridge University Press: Cambridge, UK; New York, NY, USA, 2001; p. 881.
4. Stocks, B.J.; Fosberg, M.A.; Lynham, T.J.; Mearns, L.; Wotton, M.; Yang, Q.; Jin, J.-Z.; Lawrence, K.; Hartley, G.R.; Mason, J.A.; et al. Climate change and forest fire potential in Russian and Canadian boreal forests. *Clim. Chang.* **1998**, *38*, 1–13. [CrossRef]
5. Shaver, G.R.; Canadell, J.G.; Chapin, F.S.; Gurevitch, J.; Harte, J.; Henry, G.; Ineson, P.; Jonasson, S.; Melillo, J.; Pitelka, L.; et al. Global warming and terrestrial ecosystems: A conceptual framework for analysis. *Bioscience* **2000**, *50*, 871–882. [CrossRef]
6. Stavig, L.; Collins, L.; Hager, C.; Herring, M.; Brown, E.; Locklar, E. The effects of climate change on Cordova, Alaska on the Prince William Sound. Alaska Tsunami Papers. The National Ocean Sciences Bowl. 2005. Available online: https://seagrant.uaf.edu/nosb/papers/2005/cordova-nurds.html (accessed on 23 April 2014).
7. The First Generation Coupled Global Climate Model. Available online: https://www.ec.gc.ca/ccmac-cccma/default.asp?lang=En&n=540909E4-1 (accessed on 24 September 2020).
8. Kargel, J.S.; Abrams, M.J.; Bishop, M.P.; Bush, A.; Hamilton, G.; Jiskoot, H.; Kääb, A.; Kieffer, H.H.; Lee, E.M.; Paul, F.; et al. Multispectral imaging contributions to global land ice measurements from space. *Remote Sens. Environ.* **2005**, *99*, 187–219. [CrossRef]
9. Oerlemans, J. Extracting a Climate Signal from 169 Glacier Records. *Science* **2005**, *308*, 675–677. [CrossRef]

10. Shahgedanova, M.; Stokes, C.R.; Gurney, S.D.; Popovnin, V. Interactions between mass balance, atmospheric circulation, and recent climate change on the Djankuat Glacier, Caucasus Mountains, Russia. *J. Geophys. Res.* **2005**, *110*, 1–12. [CrossRef]
11. Dong, P.; Wang, C.; Ding, J. Estimating glacier volume loss used remotely sensed images, digital elevation data, and GIS modelling. *Int. J. Remote Sens.* **2013**, *34*, 8881–8892. [CrossRef]
12. Xie, X.; Li, Y.X.; Li, R.; Zhang, Y.; Huo, Y.; Bao, Y.; Shen, S. Hyperspectral characteristics and growth monitoring of rice (*Oryza sativa*) under asymmetric warming. *Int. J. Remote Sens.* **2013**, *34*, 8449–8462. [CrossRef]
13. Elfarrak, H.; Hakdaoui, M.; Fikri, A. Development of Vulnerability through the DRASTIC Method and Geographic Information System (GIS) (Case Groundwater of Berrchid), Morocco. *J. Geogr. Inf. Syst.* **2014**, *6*, 45–58. [CrossRef]
14. Nistor, M.M.; Petcu, I.M. Quantitative analysis of glaciers changes from Passage Canal based on GIS and satellite images, South Alaska. *Appl. Ecol. Environ. Res.* **2015**, *13*, 535–549.
15. Yan, B.; Fang, N.F.; Zhang, P.C.; Shi, Z.H. Impacts of land use change on watershed streamflow and sediment yield: An assessment using hydrologic modelling and partial least squares regression. *J. Hydrol.* **2013**, *484*, 26–37.
16. Collins, D.N. Climatic warming, glacier recession and runoff from alpine basins after the little ice age maximum. *Ann. Glaciol.* **2008**, *48*, 119–124.
17. Hidalgo, H.G.; Das, T.; Dettinger, M.D.; Cayan, D.R.; Pierce, D.W.; Barnett, T.P.; Bala, G.; Mirin, A.; Wood, A.W.; Bonfils, C.J.W.; et al. Detection and attribution of streamflow timing changes to climate change in the western United States. *J. Clim.* **2009**, *22*, 3838–3855.
18. Piao, S.; Ciais, P.; Huang, Y.; Shen, Z.; Peng, S.; Li, J.; Zhou, L.; Liu, H.; Ma, Y.; Ding, Y.; et al. The impacts of climate change on water resources and agriculture in China. *Nature* **2010**, *467*, 43–51.
19. Penman, H.L. Natural evaporation from open water, bare soil and grass. *Proc. R. Soc. Lond. Ser. A Math. Phys. Sci.* **1948**, *193*, 120–145.
20. Turc, L. Estimation of irrigation water requirement, potential evapotranspiration: A simple climatic formula evolved up to date. *Ann. Agron.* **1961**, *12*, 13–49.
21. Hargreaves, G.A.; Samni, Z.A. Estimation of potential evapotranspiration. *J. Irrig. Drain. Div. Proc. Am. Soc. Civ. Eng.* **1982**, *108*, 223–230.
22. Thornthwaite, C.W. An approach toward a rational classification of climate. *Geogr. Rev.* **1948**, *38*, 55–94.
23. Allen, R.G.; Pereira, L.S.; Raes, D.; Smith, M. *Crop Evapotranspiration: Guidelines for Computing Crop Water Requirements*; FAO Irrigation and Drainage Paper 56; FAO: Rome, Italy, 1998; p. 300.
24. Nistor, M.M.; Mîndrescu, M. Climate change effect on groundwater resources in Emilia-Romagna region: An improved assessment through NISTOR-CEGW method. *Quat. Int.* **2019**, *504*, 214–228.
25. Vergnes, J.-P.; Habets, F. Impact of river water levels on the simulation of stream–aquifer exchanges over the Upper Rhine alluvial aquifer (France/Germany). *Hydrogeol. J.* **2018**, *26*, 2443–2457. [CrossRef]
26. Thierion, C.; Longuevergne, L.; Habets, F.; Ledoux, E.; Ackerer, P.; Majdalani, S.; Leblois, E.; Lecluse, S.; Martin, E.; Queguiner, S.; et al. Assessing the water balance of the Upper Rhine Graben hydrosystem. *J. Hydrol.* **2012**, *424*, 68–83. [CrossRef]
27. Kottek, M.; Grieser, J.; Beck, C.; Rudolf, B.; Rubel, F. World Map of the Köppen-Geiger climate classification updated. *Meteorol. Z.* **2006**, *15*, 259–263. [CrossRef]
28. Hamann, A.; Wang, T.; Spittlehouse, D.L.; Murdock, T.Q. A comprehensive, high-resolution database of historical and projected climate surfaces for western North America. *Bull. Am. Meteorol. Soc.* **2013**, *94*, 1307–1309. [CrossRef]

29. IPCC. Summary for Policymakers. Climate Change 2013: The Physical Science Basis. In *Contribution of Working Group I to the Fifth Assessment Report of the Intergovernmental Panel on Climate Change*; Stocker, T.F., Qin, D., Plattner, G.-K., Tignor, M., Allen, S.K., Boschung, J., Nauels, A., Xia, Y., Bex, V., Midgley, P.M., Eds.; Cambridge University Press: Cambridge, UK; New York, NY, USA, 2013; p. 1308.
30. Daly, C.; Halbleib, M.; Smith, J.I.; Gibson, W.P.; Doggett, M.K.; Taylor, G.H.; Curtis, J. Physiographically-sensitive mapping of temperature and precipitation across the conterminous United States. *Int. J. Climatol.* **2006**, *28*, 2031–2064. [CrossRef]
31. Hamann, A.; Wang, T.L. Models of climatic normals for genecology and climate change studies in British Columbia. *Agric. For. Meteorol.* **2005**, *128*, 211–221. [CrossRef]
32. Mbogga, M.S.; Hamann, A.; Wang, T. Historical and projected climate data for natural resource management in western Canada. *Agric. For. Meteorol.* **2009**, *149*, 881–890. [CrossRef]
33. Wang, T.; Hamann, A.; Spittlehouse, D.L.; Carroll, C. Locally downscaled and spatially customizable climate data for historical and future periods for North America. *PLoS ONE* **2016**, *11*, e156720. [CrossRef]
34. Dezsi, Ş.; Mîndrescu, M.; Petrea, D.; Rai, K.P.; Hamann, A.; Nistor, M.M. High-resolution projections of evapotranspiration and water availability for Europe under climate change. *Int. J. Climatol.* **2018**, *38*, 3832–3841. [CrossRef]
35. Haidu, I.; Nistor, M.M. Long-term effect of climate change on groundwater recharge in the Grand Est region, France. *Meteorol. Appl.* **2019**, *27*, e1796. [CrossRef]
36. Haidu, I.; Nistor, M.M. Groundwater vulnerability assessment in the Grand Est region, France. *Quat. Int.* **2019**, *547*, 86–100. [CrossRef]
37. Grimmond, C.S.B.; Oke, T.R. Evapotranspiration Rates in Urban Areas, Impacts of Urban Growth on SurfaceWater and Groundwater Quality. In Proceedings of the IUGG 99 Symposium HSS, Birmingham, UK, 18–30 July 1999.
38. Budyko, M.I. *Climate and Life*; Academic Press: New York, NY, USA, 1974; p. 508.
39. Gerrits, A.M.J.; Savenije, H.H.G.; Veling, E.J.M.; Pfister, L. Analytical derivation of the Budyko curve based on rainfall characteristics and a simple evaporation model. *Water Resour. Res.* **2009**, *45*, 160. [CrossRef]
40. Celico, P. *Prospezioni Idrogeologiche*; Liguori Editore Srl: Napoli, Italy, 1988; Volume II, p. 521. (In Italian)
41. Cianflone, G.; Dominici, R.; Viscomi, A. Potential recharge estimation of the Sibari plain aquifers (Southern Italy) through a new GIS procedure. *Geogr. Tech.* **2015**, *10*, 8–18.
42. Civita, M.; De Maio, M. Mapping groundwater vulnerability by the point count system model SINTACS. In *Managing Hydrogeological Disasters in a Vulnerable Environment*; Andah, K., Ed.; IHPUNESCO: Perugia, Italy, 1998; pp. 243–273.
43. BGR & UNESCO. International Hydrogeological Map of Europe (IHME1500) 1:1,500,000. International Association of Hydrogeologists 2013. Available online: http://www.bgr.bund.de/ihme1500/ (accessed on 12 September 2019).
44. Wochna, A.; Lange, K.; Urbanski, J. The influence of land cover change during sixty years on non point source phosphorus loads to Gulf of Gdansk. *J. Coast. Res.* **2011**, *64*, 1820–1824.
45. Copernicus Land Monitoring Services. CORINE Land Cover of Europe 2012. Available online: http://land.copernicus.eu/ (accessed on 21 July 2016).
46. Schulp, C.J.E.; Tieskens, K.F.; Sturck, J.; Fuchs, R.; van der Zanden, E.H.; Schrammeijer, E.; Verburg, P.H. EU Scale Analysis of Future Cultural Landscape Dynamics. Report no. 1, WP 5 Fine- and Broad-Scale Modelling of Future Landscapes. 2015. Available online: http://www.hercules-landscapes.eu/tartalom/HERCULES_WP5_D5_2_VUIVM.pdf (accessed on 3 August 2019).
47. Čenčur Curk, B.; Žvab Rožič, P.; Nistor, M.M.; Vrhovnik, P.; Verbovšek, T.; Kotelic, B.; Babic, D.; Karleuša, B.; Radman, I.; Matic, B.B.; et al. Regional water resources availability and vulnerability. In *DRINK Adria Project, Technical Report*; University of Ljubljana: Ljubljana, Slovenia, 2016.
48. Zenodo Platform. Grand Est GIS Data Layers. Available online: https://zenodo.org/record/4039849#.X2sxnGhKhPY (accessed on 21 September 2020).
49. Galleani, L.; Vigna, B.; Banzato, C.; Lo Russo, S. Validation of a Vulnerability Estimator for Spring Protection Areas: The VESPA index. *J. Hydrol.* **2011**, *396*, 233–245. [CrossRef]
50. Čenčur Curk, B.; Cheval, S.; Vrhovnik, P.; Verbovšek, T.; Herrnegger, M.; Nachtnebel, H.P.; Marjanović, P.; Siegel, H.; Gerhardt, E.; Hochbichler, E.; et al. CC-WARE Mitigating Vulnerability of Water Resources under

Climate Change. WP3—Vulnerability of Water Resources in SEE, Report Version 5. 2014. Available online: www.ccware.eu/output-documentation/output-wp3.html (accessed on 24 September 2020).
51. Nistor, M.M.; Dezsi, Ș.; Cheval, S. Vulnerability of groundwater under climate change and land cover: A new spatial assessment method applied on Beliş district (Western Carpathians, Romania). *Environ. Eng. Manag. J.* **2015**, *14*, 2959–2971.
52. Kløve, B.; Ala-Aho, P.; Bertrand, G.; Gurdak, J.J.; Kupfersberger, H.; Kværner, J.; Muotka, T.; Mykrä, H.; Preda, E.; Rossi, P.; et al. Climate change impacts on groundwater and dependent ecosystems. *J. Hydrol.* **2014**, *518*, 250–266.
53. Cisneros, B.E.J.; Oki, T.; Arnell, N.W.; Benito, G.; Cogley, J.G.; Döll, P.; Jiang, T.; Mwakalila, S.S. Freshwater resources. Climate Change 2014: Impacts, Adaptation, and Vulnerability. Part A: Global and Sectoral Aspects. In *Contribution of Working Group II to the Fifth Assessment Report of the Intergovernmental Panel on Climate Change*; Field, C.B., Barros, V.R., Dokken, D.J., Mach, K.J., Mastrandrea, M.D., Bilir, T.E., Chatterjee, M., Ebi, K.L., Estrada, Y.O., Genova, R.C., Eds.; Cambridge University Press: Cambridge, UK; New York, NY, USA, 2014; pp. 229–269.
54. Aguilera, H.; Murillo, J.M. The effect of possible climate change on natural groundwater recharge based on a simple model: A study of four karstic aquifers in SE Spain. *Environ. Geol.* **2009**, *57*, 963–974. [CrossRef]
55. Yan, Y.; Zhou, J.; He, Z.; Sun, Q.; Fei, J.; Zhou, X.; Zhao, K.; Yang, L.; Long, H.; Zheng, H. Evolution of Luyang Lake since the last 34,000 years: Climatic changes and anthropogenic impacts. *Quat. Int.* **2017**, *440*, 90–98. [CrossRef]
56. Ghazavi, R.; Ebrahimi, Z. Assessing groundwater vulnerability to contamination in an arid environment using DRASTIC and GOD models. *Int. J. Environ. Sci. Technol.* **2015**, *12*, 2909–2918. [CrossRef]
57. Nistor, M.M.; Nicula, A.S.; Cervi, F.; Man, T.C.; Irimuș, I.A.; Surdu, I. Groundwater vulnerability GIS models in the Carpathian Mountains under climate and land cover changes. *Appl. Ecol. Environ. Res.* **2018**, *16*, 5095–5116. [CrossRef]
58. Stempvoort, D.V.; Ewert, L.; Wassenaar, L. Aquifers vulnerability index: A GIS—Compatible method for groundwater vulnerability mapping. *Can. Water Resour. J. Rev. Can. Ressour. Hydr.* **1993**, *18*, 25–37. [CrossRef]
59. Wright, C.Y.; Norval, M.; Kapwata, T.; du Preez, D.J.; Wernecke, B.; Tod, B.M.; Visser, W.I. The incidence of skin cancer in relation to climate change in South Africa. *Atmosphere* **2019**, *10*, 634. [CrossRef]
60. Andrade, L.; O'Dwyier, J.; O'Neill, E.; Hynds, P. Surface water flooding, groundwater contamination, and enteric disease in developed countries: A scoping review of connections and consequences. *Environ. Pollut.* **2018**, *236*, 540–549. [CrossRef]
61. Sterk, A.; Schijven, J.; de Nijs, T.; de Roda Huisman, A.M. Direct and indirect effects of climate changeon the risk of infection by water-transmitted pathogens. *Environ. Sci. Technol.* **2013**, *47*, 12648–12660. [CrossRef]
62. Prueksapanich, P.; Piyachaturawat, P.; Aumpansub, P.; Ridtitid, W.; Chaiteerakij, R.; Rerknimitr, R. Liver fluke-associated biliary tract cancer. *Gut Liver* **2018**, *12*, 236–245. [CrossRef]